

MSCoTDet: Language-driven Multi-modal Fusion for Improved Multispectral Pedestrian Detection

Taeheon Kim^{*1}, Sangyun Chung^{*1}, Damin Yeom¹, Youngjoon Yu¹, Hak Gu Kim²,
and Yong Man Ro^{†1}

¹ Integrated Vision and Language Lab, KAIST, South Korea

{eetaekim, jelarum, damin321, greatday, ymro}@kaist.ac.kr

² Immersive Reality and Intelligent Systems Lab, Chung-Ang University, South Korea
hakgukim@cnu.ac.kr

Abstract. Multispectral pedestrian detection is attractive for around-the-clock applications due to the complementary information between RGB and thermal modalities. However, current models often fail to detect pedestrians in obvious cases, especially due to the modality bias learned from statistically biased datasets. From these problems, we anticipate that maybe understanding the complementary information itself is difficult to achieve from vision-only models. Accordingly, we propose a novel Multispectral Chain-of-Thought Detection (MSCoTDet) framework, which incorporates Large Language Models (LLMs) to understand the complementary information at the semantic level and further enhance the fusion process. Specifically, we generate text descriptions of the pedestrian in each RGB and thermal modality and design a Multispectral Chain-of-Thought (MSCoT) prompting, which models a step-by-step process to facilitate cross-modal reasoning at the semantic level and perform accurate detection. Moreover, we design a Language-driven Multi-modal Fusion (LMF) strategy that enables fusing vision-driven and language-driven detections. Extensive experiments validate that MSCoTDet improves multispectral pedestrian detection.

Keywords: Multispectral Chain-of-Thought Detection · Language-driven Multi-modal Fusion · Multispectral Pedestrian Detection · Large Language Model

1 Introduction

Multispectral pedestrian detection is the task of detecting pedestrians based on different visual modalities (i.e., RGB and thermal) [20, 30, 33, 37, 40, 62, 66, 67]. Due to their complementary information, combining these modalities improves pedestrian detection all day/night [26, 28, 70]. With the advances in this field, the primary interest in multispectral pedestrian detection has been focused on how to effectively fuse the complementary information between the two modalities. Previous works investigated various fusion methods in different stages of the network, which are often categorized as early-fusion [57], mid-fusion [29, 31, 50], and late-fusion [9, 57]. These methods demonstrated superior detection performance compared to standard pedestrian detection [15, 21, 25, 32], especially in practical datasets that contain all day/night scenarios.

^{*} Equally contributed.

[†] Corresponding author.

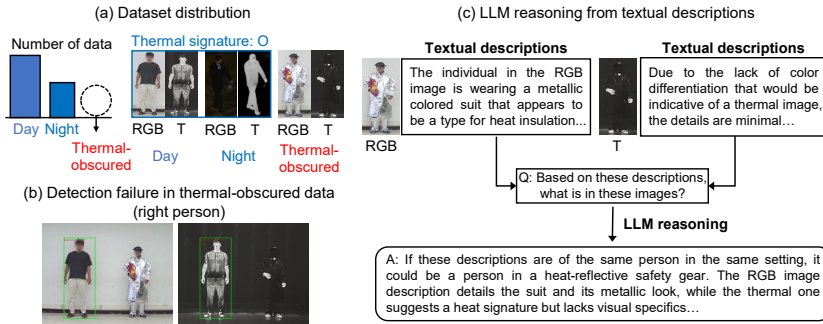


Fig. 1: Problem illustration and our motivation. (a) In multispectral pedestrian datasets, thermal signatures always appear on pedestrians, as the thermal modality can generally capture pedestrians all day/night. In these datasets, thermal-obscured data is underrepresented. Models trained on such datasets learn the statistical co-occurrences between pedestrians and their thermal signatures. (b) As a result, models fail to detect pedestrians in thermal-obscured data, even though obviously visible in RGB. (c) Our motivation is to use Large Language Models (LLMs) to correctly combine complementary information of RGB and thermal, and intervene in modality bias.

Despite the progress in this task, there are still remaining problems that need to be solved. From a recent study [14, 31], multispectral pedestrian detection models are known to suffer from modality bias toward the thermal modality, due to learning the statistical bias in datasets. In multispectral pedestrian datasets, pedestrians always statistically co-occur with their thermal signatures [31] as the thermal modality is generally robust all day/night. Models trained on these datasets learn the statistical co-occurrences of thermal signatures on pedestrians and detect pedestrians based on the presence of thermal signatures. As a result, models often fail to detect pedestrians that have weak thermal signatures (i.e., thermal-obscured pedestrians), even though they are obviously visible in RGB [31]. This phenomenon, also illustrated in Fig. 1, indicates that models often fail to correctly fuse the complementary information between the two modalities.

We anticipate that understanding the complementary information itself may be difficult to achieve from vision-only models because it requires a high level of understanding of the intra- and inter-modality contexts at the semantic level. On the other hand, language models are known to understand the semantic contexts between different modalities [1, 7, 27] (e.g., image and text [69]) and elicit correct reasoning steps required for completing tasks [16, 51, 58, 59, 68]. If the contextual elements (e.g., object category names, attributes, and the overall scene) of different visual modalities can be represented in the same semantic space through textual descriptions, Large Language Models (LLMs) [4, 10, 24, 46, 54, 60] can use their semantic understanding capabilities to comprehend the context within intra- and inter-modalities. Moreover, as language models are excellent few-shot learners that can perform complex reasoning tasks [4, 55], a few task-specific exemplars can expand their general knowledge to complete the task.

Based on these motivations, we propose the Multispectral Chain-of-Thought Detection (MSCoTDet) framework, which incorporates Large Language Models (LLMs) to enhance the fusion process. Specifically, MSCoTDet consists of three parts: the vision branch, the language branch, and the Language-driven Multi-modal Fusion

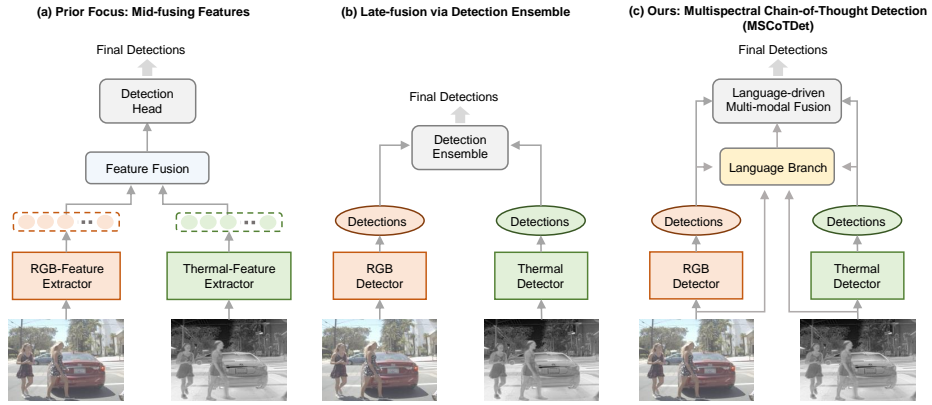


Fig. 2: Comparisons between previous works and our method (MSCoTDet). (a) Previous approaches centrally focused on mid-fusion methods, e.g., mid-fusing features internally in the network. (b) There are few works via late fusion that ensemble detections from independently trained single-modal detectors, i.e., RGB and thermal detectors. (c) MSCoTDet (Ours) focuses on designing a language branch that processes detection using Large Language Models (LLMs). Then, our proposed Language-driven Multi-modal Fusion (LMF) enables fusing vision-driven and language-driven detections.

(LMF). First, the vision branch consists of single-modal detectors of the RGB and thermal modalities. Second, the language branch first generates text descriptions of pedestrians detected in the vision branch, utilizing Multi-modal Language Models (MLLMs) [1, 13, 39, 71]. The key idea of MSCoTDet is the proposed Multispectral Chain-of-Thought (MSCoT) prompting, human-like strategic reasoning inspired by the Chain-of-Thought [59] prevalent in LLMs. Using textual descriptions from MLLMs, MSCoT first makes a decision based on a single modality. Then, MSCoT makes logical deductions by building cross-modal reasoning according to decisions from both modalities. This ability to generate rationale across modalities is similar to human cognitive processes, where different sensory streams are integrated into the parietal cortex [3, 11, 12] to form a cohesive understanding of the whole perception. By facilitating cross-modal reasoning using LLMs, MSCoT can achieve accurate detection by intervening in modality biases like humans do. Then, LMF can finally integrate the fused detections from both the vision and language branches. Extensive experiment results show that our proposed method can intervene in modality bias and improve the overall performance of multispectral pedestrian detection models.

The main contributions of our paper are:

1. To the best of our knowledge, this is the first work to integrate the Large Language Models (LLMs) in multispectral pedestrian detection.
2. We propose the Multispectral Chain-of-Thought Detection (MSCoTDet) framework, which models a step-by-step process to facilitate cross-modal reasoning at the semantic level and perform accurate detection.
3. We propose Language-driven Multi-modal Fusion (LMF), a strategy that enables the fusion of vision-driven detections and language-driven detections.

4. Extensive experiments demonstrate that our proposed method can significantly mitigate the modality bias and improve the overall performance of multispectral pedestrian detectors.

2 Preliminaries

Before introducing our method, we review the late-fusion strategies in multispectral pedestrian detection.

2.1 Late-fusion in Multispectral Pedestrian Detection

Rather than fusing modalities in the input stage (early-fusion [43, 53, 56]) or in the intermediate steps (mid-fusion [28, 50]), late-fusion [8, 9] is based on detection ensembling, i.e., fusing the decision values. One of the advantages of late fusion is that it can preserve single-modal models and, therefore, has high flexibility to perform multi-modal fusion from diverse models of different modalities [8, 23, 42, 47, 52, 63].

Late fusion methods have been also investigated in multispectral pedestrian detection [9]. They first train single-modal detectors (i.e., RGB and thermal) and then fuse the prediction scores (score fusion) and bounding boxes (box fusion) which are the outputs from single-modal detectors. The final output includes fused prediction scores and bounding boxes. We describe score fusion and box fusion strategies below.

Score Fusion. The most common strategies to fuse prediction scores obtained from single-modal models are averaging [37, 40], Non-maximum Suppression (NMS) [9], and Probabilistic Ensembling (ProbEn [9]). Between them, we adapt averaging and NMS, as we find them effective for our method (Section 3.4). Averaging is straightforward, the fused score is determined by averaging prediction scores estimated in each modality. Denote s_{RGB} and s_T the prediction scores predicted for the same object in different modalities (i.e., RGB and thermal). Then the averaging score fusion between s_{RGB} and s_T can be expressed as:

$$s_{AVG} = \frac{s_{RGB} + s_T}{2}, \quad (1)$$

where s_{AVG} denotes the fused score. On the other hand, NMS compares the prediction scores estimated in each modality and votes for the highest one, removing the lower scores. NMS score fusion between s_{RGB} and s_T can be expressed as:

$$s_{NMS} = \max(s_{RGB}, s_T), \quad (2)$$

where s_{NMS} denotes the fused score by the NMS.

Box Fusion. Box fusion is to merge overlapping bounding boxes predicted from different modalities (i.e., RGB and thermal). Chen et al.(2022) [9] suggests a simple and effective way to probabilistically fuse boxes, which computes a weighted average of boxes. The weights are given by the prediction scores, implying that more confident detections should have a higher weight when fusing boxes. Denote b_{RGB} and b_T the bounding box coordinates predicted for the same object in different modalities (i.e.,

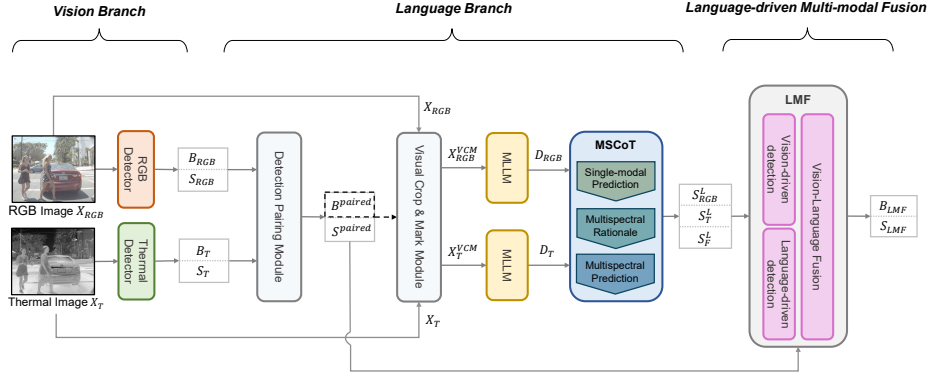


Fig. 3: Overall architecture of proposed Multispectral Chain-of-Thought detection (MSCoTDet) framework including vision branch, language branch, and language-driven multi-modal fusion.

RGB and thermal). Using the predictions scores s_{RGB} , and s_T , the weighted-averaging box fusion between b_{RGB} and b_T can be expressed as:

$$b_{s-avg} = \frac{b_{RGB} \times s_{RGB} + b_T \times s_T}{s_{RGB} + s_T}, \quad (3)$$

where b_{s-avg} denotes the fused bounding boxes.

3 Proposed Method

3.1 Overall Architecture

The overall architecture of our proposed pedestrian detection network is shown in Fig. 3. It consists of two branches that perform distinct detection processes, the vision branch and the language branch. Detections from these branches are fused to output final detections. We briefly introduce the process of each branch and our fusion strategy.

Vision branch. Given the input of RGB and thermal images X_{RGB} and X_T , the vision branch first produces single-modal (i.e., RGB or thermal) detections. Denote the prediction scores as S_{RGB} , S_T and bounding boxes as B_{RGB} , B_T produced from each single-modal detector. The single-modal detections in the vision branch are processed through the language branch.

Language Branch. The language branch first generates text descriptions of pedestrians and performs detections based on them. Toward this goal, we leverage Multi-modal Large Language Models (MLLMs), which are capable of generating comprehensive descriptions in both RGB and thermal images. Based on these descriptions, we propose the Multispectral Chain-of-Thought (MSCoT) prompting, which prompts the LLM to conduct reasoning steps and produce detections (Section 3.3). Detections from MSCoT include single-modal (i.e., RGB and thermal) prediction scores S_{RGB}^L , S_T^L , and fused prediction scores S_F^L . In Sections 3.2 and 3.3, we describe the processes to produce these detections in detail.

Language-driven Multi-modal Fusion (LMF). Vision-driven detection, language-driven detection, and vision-language fusion are performed to produce final detections, S_{LMF} and B_{LMF} . In Section 3.4, we describe the fusion strategies in detail.

3.2 Cross-modal Pedestrian Description Generation

The first step of the language branch is to generate text descriptions of pedestrians, both from the RGB and thermal images. We prompt Multi-modal Large Language Models (MLLMs [1]) to describe pedestrian regions in the image, which can be identified by their bounding box coordinates B_{RGB} , B_T obtained from single-modal detectors. However, there are two challenges, which we introduce below with their solutions.

Detection Pairing. The first challenge is due to the misalignment in multispectral data [26, 29]. The same pedestrian often appears in different locations within the RGB and thermal image pairs, as their image sensors may have different Field-of-View or frame rates [29]. Thus sometimes we need to guide MLLMs to make descriptions based on different image regions in RGB and thermal images for the same pedestrians. Our strategy is to find the detection pairs from the single-modal detections (e.g., bounding boxes) that belong to the same pedestrians and provide this information to the MLLM.

Although bounding boxes representing the same pedestrian can have different coordinates in different modalities, still they will contain highly overlapping areas in the images, and those boxes will have large values of IoUs (Intersection-of-Unions). Specifically, for the i -th bounding box $b_{i,m}$ in bounding boxes B_m , obtained from the single-modal detector in the m modality (m is either RGB or thermal: T), we aim to find the bounding box from B_{m^c} , in the opposite modality m^c that corresponds to the same pedestrian. To this end, we compute the IoU value between $b_{i,m}$ across all bounding boxes in B_{m^c} , and find the box that has the highest IoU value, e.g., b_{j,m^c} , with $b_{i,m}$. Here, we only consider the boxes with IoU values above the IoU threshold τ . With indices i and j , we can find a pair of the prediction scores $s_{i,m}$ and s_{j,m^c} that belong to the same pedestrian. We call such tuples $(b_{i,m}, b_{j,m^c})$ and $(s_{i,m}, s_{j,m^c})$ as the "paired detection". When all IoU values are under the IoU threshold τ , this means that there are no boxes in B_{m^c} that correspond to the same pedestrian and $b_{i,m}$ can not find a pair. Such cases can occur at nighttime or in thermal-obscured scenarios where the pedestrian is detected by only one modality. In this case, we override the value of $b_{i,m}$ and $s_{i,m}$ to the opposite modality, making pairs of $(b_{i,m}, b_{i,m})$ and $(s_{i,m}, s_{i,m})$. Iterating this process for over all bounding boxes in B_m and B_{m^c} (i.e., B_{RGB} and B_T) allows us to obtain a set of paired detections B^{paired} and S^{paired} . Denote the Detection Pairing Module as a function $DPair(\cdot)$ with respect to inputs B_{RGB} , B_T , S_{RGB} , and S_T , which indicate bounding boxes and prediction scores obtained from RGB and thermal single-modal detectors, respectively. The inputs and outputs of $DPair(\cdot)$ can be represented as:

$$S^{paired}, B^{paired} = DPair(B_{RGB}, B_T, S_{RGB}, S_T; \tau), \quad (4)$$

where τ indicates an IoU threshold. We set this value to 0.5, the standard value used in the object detection task. B^{paired} is used to guide MLLMs the location of when making descriptions in RGB and thermal images. S^{paired} is used when fusing prediction scores from vision and language branches in Section 3.4. The complete algorithm of the Detection pairing Module is described in Algorithm 2 in the supplementary material.

Visual Crop & Mark (VCM). Another challenge when using MLLMs for making descriptions is the low accuracy of MLLMs on small-scale objects, i.e., objects occupying a small area in the image. To solve this issue, we refer to a recent method [65] that improves the performance of MLLMs on small visual details by pre-processing the

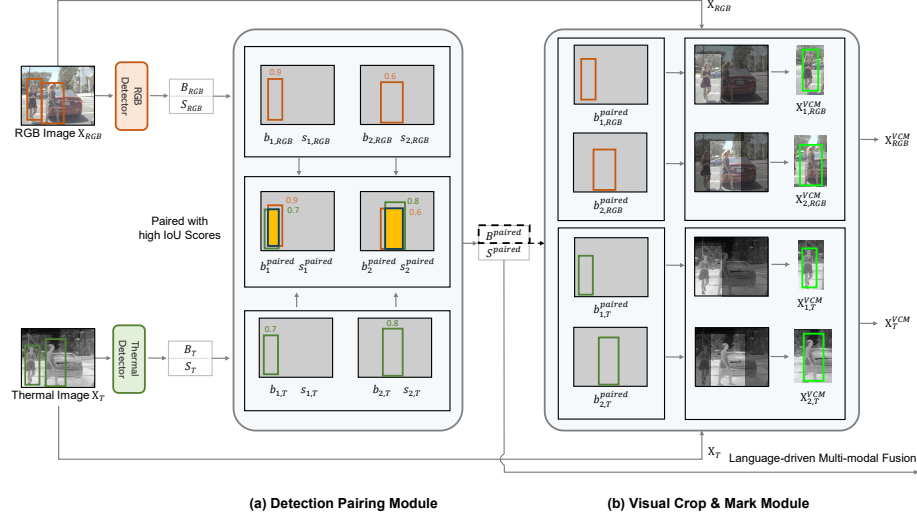


Fig. 4: Visualized details of the (a) Detection Pairing Module and the (b) Visual Crop & Mark Module. (a) The Detection Pairing Module gets single-modal detections from the vision branch and then finds the detection pairs that belong to the same pedestrians, e.g., $b_1^{paired} = (b_{1,RGB}^{paired}, b_{1,T}^{paired})$ and $s_1^{paired} = (s_{1,RGB}^{paired}, s_{1,T}^{paired})$. Through the iteration of pedestrians, the module produces the sets of paired detections B^{paired} and S^{paired} . (b) The Visual Crop & Mark Module gets B^{paired} as inputs, and output the sets of pre-processed images X_{RGB}^{VCM} and X_T^{VCM} .

input image with image cropping. Similarly, we zoom in on the target pedestrians and crop the image around it, such that visual information irrelevant to the pedestrian is removed. We find such a pre-processing strategy is shown to significantly improve the accuracy of MLLMs in describing small-scale pedestrians, near the level comparable to recognizing large-scale pedestrians. Since the process requires simple image cropping processes, we elaborate on the details in the supplementary material.

In addition to cropping, we visually guide the MLLM to describe a specific pedestrian by drawing a 1-pixel width "green" color (with RGB values (0,255,0)) box around a target pedestrian. We use the "green" color to draw the boxes because it is most distinctly in hue from human skin color, thus effective for distinguishing humans from the background. Denote this the Visual Crop & Mark process as $VCM(\cdot)$, then the pre-processed RGB and thermal images X_{RGB}^{VCM} and X_T^{VCM} can be written as:

$$X_{RGB}^{VCM} \leftarrow VCM(X_{RGB}, B^{paired}), X_T^{VCM} \leftarrow VCM(X_T, B^{paired}), \quad (5)$$

where X_{RGB} and X_T are RGB and thermal input images, and B^{paired} is the set of the paired bounding boxes. When pre-processing images in X_{RGB} and X_T , bounding boxes of the corresponding modality in B^{paired} are used only.

Generating Descriptions with MLLMs. For each pre-processed image $x_{RGB}^{VCM} \in X_{RGB}^{VCM}$ and $x_T^{VCM} \in X_T^{VCM}$, we prompt the MLLM as the following. For the RGB image, "In this RGB image, what is in the green box?" and for the thermal image, "In this thermal image, what is in the green box?". Denote these prompts as p_{RGB} , and p_T .

Then, we can generate their corresponding text descriptions d_{RGB} and d_T such as:

$$d_{RGB} \leftarrow MLLM(x_{RGB}^{VCM}; p_{RGB}), d_T \leftarrow MLLM(x_T^{VCM}; p_T), \quad (6)$$

where $MLLM(\cdot)$ denotes the process of generating text descriptions from an MLLM, given the pre-processed image as input. Text descriptions are generated for all $x_{RGB}^{VCM} \in X_{RGB}^{VCM}$ and $x_T^{VCM} \in X_T^{VCM}$, producing sets of descriptions D_{RGB} and D_T .

3.3 Multispectral Chain-of-Thought Prompting

A complex reasoning process is required to properly use the complementary information of the RGB and thermal modalities based on their textual information. Our key idea is to leverage LLM’s semantic understanding capabilities to model reasoning steps to complete the task. To this end, we refer to the Chain-of-Thought (CoT) prompting [59] technique, which significantly improves LLM’s reasoning ability in complex NLP tasks. CoTs add a series of intermediate reasoning steps into LLMs and generate rationales when predicting answers. Motivated by the late-fusion process in multispectral pedestrian detection, we propose a Multispectral Chain-of-Thought (MSCoT) prompting chain. Given the text descriptions $d_{RGB} \in D_{RGB}$ and $d_T \in D_T$ of a RGB image and a thermal image, MSCoT first prompts the LLM to produce single-modal prediction scores s_{RGB}^L , and s_T^L and then predict a fused prediction score s_F^L based on rationale chains. Given the descriptions d_{RGB} , and d_T of RGB and thermal images as the context, we design the following prompt chains:

Generating Single-modal Prediction.

Context: RGB image description d_{RGB} , thermal image description d_T .

Prompt: First, predict what is in the RGB image based on d_{RGB} . And predict what is in the thermal image based on d_T . Please answer in the format : [class, prediction score]

From the above prompt, the LLM outputs single-modal prediction scores s_{RGB}^L , and s_T^L . Additionally providing s_{RGB}^L , and s_T^L as the context, the following prompts for generating fused prediction scores and multispectral rationales are:

Generating Multispectral Rationales and Prediction.

Context: RGB image description: d_{RGB} , thermal image description: d_T , answers: s_{RGB}^L , and s_T^L .

Prompt: Based on the descriptions and your answers, predict what is in these aligned RGB and thermal images. Please answer in the format: [class, prediction score]

Then the LLM outputs fused prediction scores s_F^L . For all steps, the prediction scores s_{RGB}^L , s_T^L , and s_F^L are assigned only if the class outputs are "Person". If not, the prediction scores are assigned as zero. Our implementation for MSCoT is achieved by fine-tuning ChatGPT-3.5 [44] with about 50 training samples. The implementation details are described in detail in Section 4.2.

$$s_{RGB}^L, s_T^L, s_F^L = MSCoT(d_{RGB}, d_T). \quad (7)$$

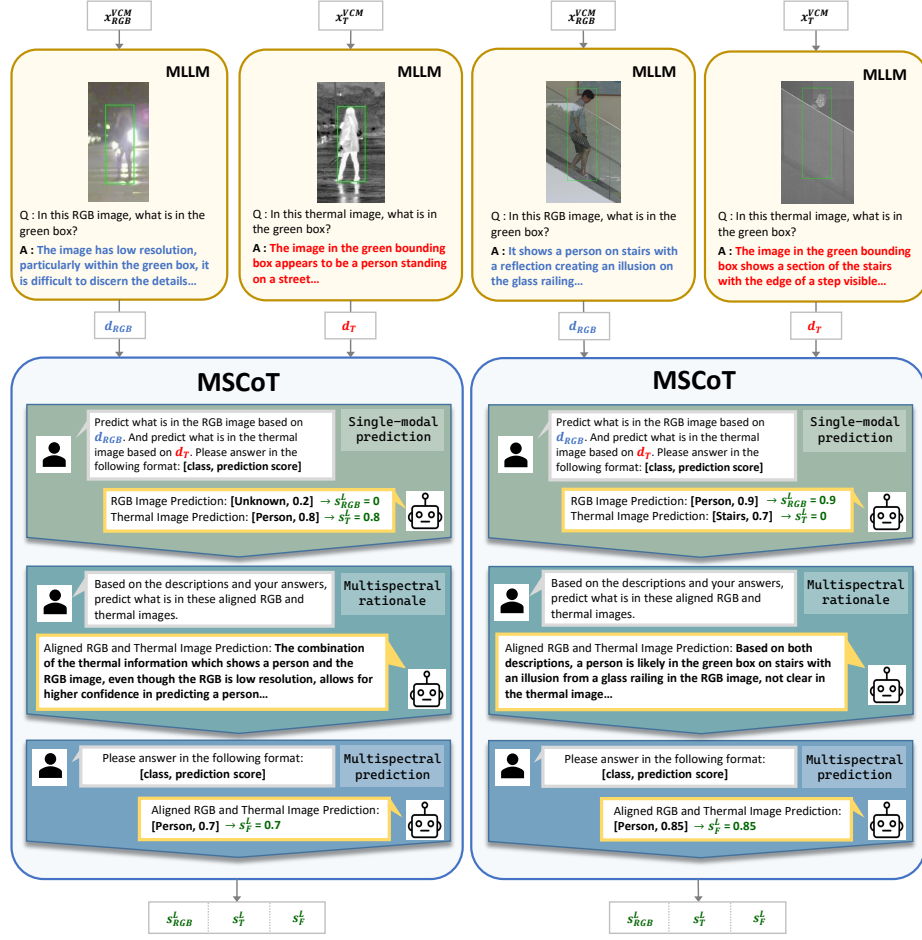


Fig. 5: Visualized process of our proposed Multispectral Chain-of-Thought (MSCoT) prompting.

Iterating this process over all $d_{RGB} \in D_{RGB}$ and $d_T \in D_T$ obtains the prediction scores: S_{RGB}^L , S_T^L , and S_F^L .

3.4 Language-driven Multi-modal Fusion (LMF)

We propose to ensemble the detections of the vision branch and the language branch at the last stage of the proposed network (Fig. 3).

Vision-driven Detection. For the vision branch, denote S_{RGB}^V as the prediction scores from S^{paired} , and B_{RGB}^V as the bounding boxes from B^{paired} that corresponds to the RGB modality, similar for S_T^V and B_T^V . Then, the vision-driven detections S_F^V (prediction scores) and B_F^V (bounding boxes) can be produced as:

$$S_F^V = \max(S_{RGB}^V, S_T^V), B_F^V = \frac{B_{RGB}^V \odot S_{RGB}^V + B_T^V \odot S_T^V}{S_{RGB}^V + S_T^V}, \quad (8)$$

where \odot denotes the Hadamard product (element-wise multiplication). NMS (Eq. 2) and weighted-averaging (Eq. 3) are applied for score-fusion and box-fusion.

Language-driven Detection. Next, for the language branch, fused bounding boxes B_F^L can be produced as:

$$B_F^L = \frac{B_{RGB}^V \odot S_{RGB}^L + B_T^V \odot S_T^L}{S_{RGB}^L + S_T^L}, \quad (9)$$

given the bounding boxes B_{RGB}^V , B_T^V obtained single-modal detectors. Weighted-averaging (Eq. 3) is applied for box-fusion. The fused prediction scores S_F^L are produced by the MSCoT (Section 3.3).

Vision-Language Fusion. Lastly, final detections are produced as:

$$S_{LMF} = avg(S_F^V, S_F^L), \quad B_{LMF} = \frac{S_F^V \odot B_F^V + S_F^L \odot B_F^L}{S_F^V + S_F^L}, \quad (10)$$

where S_{LMF} and B_{LMF} denote final prediction scores and bounding boxes. Averaging (Eq. 2) and weighted-averaging (Eq. 3) are applied for score-fusion and box-fusion.

Design Choice. For score-fusion, we adapted the NMS method (Eq. 2) in the vision-driven detection. NMS compares the prediction scores estimated in each modality and votes for the highest one, removing the lower score. We apply such a strategy because higher confidence scores generally occur when there is more useful information for detecting the pedestrian. From this strategy, we can obtain higher prediction scores for true-positive detections in most cases. However, it can also increase the prediction scores for false positives. As MSCoT can comprehend very low prediction scores for false positives, we adapt the averaging strategy (Eq. 1) in the vision-language fusion to refine over-confident false positives from the vision-driven detections. For box-fusion, we adapted the weighting average (Eq. 3) method in all processes, implying that more confident detections should have a higher weight when fusing. In Section 6.2, we conduct an ablation study on these design choices.

4 Experimental Setup

4.1 Dataset and Evaluation Metric

The experiments are conducted on multispectral pedestrian datasets: Teledyne FLIR Free ADAS Thermal Dataset v2.0.0 [17], CVC-14 [19], ROTX-MP [31]. The FLIR [17] dataset consists of RGB and thermal image pairs with an image resolution of 640×512 . For a fair comparison with previous studies [31, 33, 49, 64], we use the aligned version of FLIR, proposed by [64]. This version filters out misaligned images, containing well-aligned 4,129 training and 1,013 test RGB and thermal image pairs. For convenience, we call this version of the dataset as FLIR. Following previous works, we evaluate both day and night images and report the performance on the entire test set ('All'). In contrast to FLIR, the CVC-14 [19] dataset often contains heavily misaligned pairs of RGB and thermal images. The train and test set each contains 3,618 and 1,433 grayscale and thermal images with a 640×471 resolution. We evaluate daytime ('Day'), nighttime ('Night'), and the total ('All') test images separately, following previous works [29, 31].

Lastly, we evaluate our method on the ROTX-MP [31] dataset, which consists of 1,000 test images of mainly thermal-obscured pedestrians. We use the models trained from FLIR and CVC-14 to test on ROTX-MP, as the purpose of this dataset is to evaluate models when there is a substantial distribution difference between the train and test splits. For the evaluation metric, we use the Average Precision (AP \uparrow). These experimental settings are the same as the original paper [31].

4.2 Implementation Detail

Single-modal Detectors. For the single-modal detectors, we use the Co-DETR [72] model and train RGB images and thermal images separately. Co-DETR is based on the DETR (DEtection TRansformer) [5] architecture, enhanced by collaborative learning with multiple parallel auxiliary heads integrated into the output of the transformer encoder. We train the single-modal detectors with RGB and thermal images from FLIR [17] and CVC-14 [19] training data, respectively. For optimizing Co-DETR, we use the same setting in the original paper [72], using AdamW [41] optimizer with an initial learning rate of $1e-4$ and weight decay of $1e-4$. All models are trained on an eight NVIDIA A6000 GPU for 16 epochs with a batch size of 16.

Large Language Models (LLMs). We use two types of Large Language Models. First is the Multimodal Large Language Model (MLLM), which we use to generate text descriptions for RGB and thermal pedestrian images (Section 3.2). For the MLLM, we use the pre-trained model of the ChatGPT-vision (GPT-4V) [1] API, provided by the OpenAI developer platform. ChatGPT-vision API service is not free, therefore we paid the company to use the service. A total of \$500 is spent for our experiments.

The second is the chatbot version, ChatGPT-3.5 (GPT-3.5) API [44], also provided by the OpenAI developer platform. We fine-tuned the GPT-3.5 model for the Multi-spectral Chain-of-Thought (MSCoT) prompting (Section 3.3) we proposed. Using the fine-tuning module provided on the GPT official website [45], we trained GPT-3.5 API with our high-quality selection pairs consisting of RGB, thermal descriptions, rationale, and prediction scores. The official document for GPT-3.5 [45] recommends training 50 samples for fine-tuning the model, and we utilized a total of 50 training samples. We provide our examples in the supplementary material.

4.3 Comparison Model

We compare our method with five multispectral pedestrian detection models: 1) Halfway Fusion [40], 2) Cross-modality Fusion Transformer (CFT) [49], 3) Kim et al. [29], 4) ProbEn [9], and 5) Causal Mode Multiplexer (CMM) [31]. For these methods, we used the same experimental settings as their original papers. More details of these methods and their settings are described in the supplementary material.

5 Experimental Result

5.1 Result on FLIR, and CVC-14

We train and test on FLIR [17], CVC-14 [19] datasets to evaluate whether our method performs well on general multispectral pedestrian data. We report the detection performance of different models on these datasets. For the evaluation metrics, we

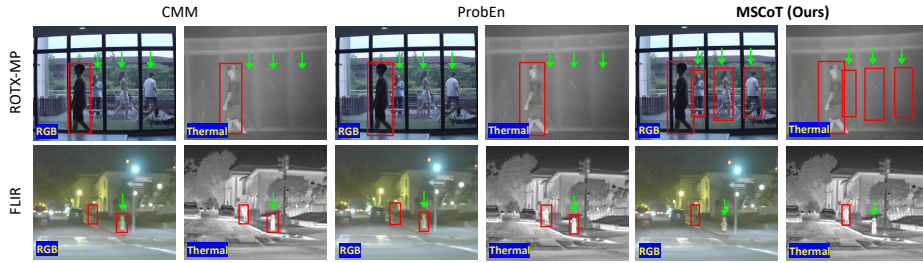


Fig. 6: Visualized detections on the ROTX-MP [31] (Top) and FLIR [17] (Bottom) datasets. (Top): MSCoTDet can detect pedestrians over the window (\downarrow), in which their thermal signatures are absent due to the window. In contrast, other models [9, 31] fail to detect these pedestrians. (Bottom): Moreover, other models [9, 31] create false-positive detections on the fireplug (\downarrow) due to its thermal signature similar-looking to pedestrians. In contrast, MSCoTDet (Ours) makes correct predictions.

Train	FLIR		CVC-14		Modality Used		
	Test	FLIR	CVC-14				
Metric	AP (\uparrow)		MR (\downarrow)				
Method	All	Day	Night	All	RGB	Thermal	Language
Halfway Fusion [40]	75.85	36.29	26.29	31.99	✓	✓	
CFT [49]	84.10	18.81	25.25	21.83	✓	✓	
Kim et al. [29]	84.67	23.87	11.08	18.7	✓	✓	
CMM [31]	87.8	27.81	7.71	17.13	✓	✓	
ProbEn [9]	86.74	23.01	21.02	22.23	✓	✓	
MSCoTDet (Ours)	90.39	6.69	13.69	10.39	✓	✓	✓

Train	FLIR		CVC-14		Modality Used		
	Test	ROTX-MP	ROTX-MP				
Metric	AP (\uparrow)		AP (\uparrow)				
Method	All	All	RGB	Thermal	Language		
Halfway Fusion [40]	36.95	8.8	✓	✓			
CFT [49]	3.64	8.58	✓	✓			
Kim et al. [29]	21.69	13.36	✓	✓			
CMM [31]	57.09	34.96	✓	✓			
ProbEn [9]	17.2	16.66	✓	✓			
MSCoTDet (Ours)	67.33	57.65	✓	✓	✓		

Table 1: Detection performance on the FLIR [17], CVC-14 [19] (Left), and ROTX-MP [31] (Right). (Left): We train and test on FLIR, CVC-14 datasets. (Right): We train models on FLIR, CVC-14, and evaluate models on the ROTX-MP dataset. We adapt this experimental setting following the original paper [31] to evaluate models when there is a substantial distribution difference between train and test sets. We compare our proposed method with different multispectral pedestrian detection models [9, 29, 31, 40, 49] recently proposed. The best results are highlighted.

follow previous studies on multispectral pedestrian detection to measure the detection performances on these datasets and make a fair comparison. Specifically, we use average precision (AP) on FLIR (‘All’). For CVC-14, we use the log-average miss rate (MR) for evaluating models and report the performance on daytime (‘Day’) and nighttime (‘Night’), and the entire set (‘All’) of images separately. Note that lower MR (MR \downarrow) and higher AP (AP \uparrow) values indicate better detection performance.

Table 1 (Left) shows the experimental results on the FLIR and CVC-14 test set. On FLIR (‘All’), MSCoTDet achieves the highest AP (90.39 AP), which outperforms other methods by at least 2.59 AP. Such results indicate the effectiveness of MSCoTDet on well-aligned data. On CVC-14, MSCoTDet demonstrates the lowest miss rate among models in (‘Day’), and (‘All’), with a value of 6.69 MR and 10.39 MR, respectively. Our method surpasses other models by at least 12.12 MR for (‘Day’) and 6.74 MR for (‘All’). As (‘All’) indicates the entire dataset, our method achieves the best performance also on CVC-14. Such results illustrate that MSCoTDet is also effective on a dataset that largely contains misaligned multispectral data.

Train	FLIR	CVC-14			Modality Used		
Test	FLIR	CVC-14					
Metric	AP (\uparrow)	MR (\downarrow)					
Method	All	Day	Night	All	RGB	Thermal	Language
RGB only	76.06	31.55	40.10	36.07	✓		
Thermal only	85.73	43.24	33.44	36.07		✓	
Late-fusion	88.60	18.33	18.86	21.57	✓	✓	
MSCoTDet (Ours)	90.39	6.69	13.69	10.39	✓	✓	✓

Train	FLIR	CVC-14		Modality Used		
Test	ROTX-MP	ROTX-MP				
Metric	AP (\uparrow)	AP (\uparrow)				
Method	All	All	All	RGB	Thermal	Language
RGB only	54.20	31.05		✓		
Thermal only	19.33	9.10			✓	
Late-fusion	58.95	44.72		✓	✓	
MSCoTDet (Ours)	67.33	57.65		✓	✓	✓

Table 2: Ablation study on the effect of using language models. Our focus is to compare MSCoTDet with ‘Late-fusion’, the vision branch equipped with vision-driven detection of MSCoTDet.

5.2 Result on ROTX-MP

Experimenting with models on the ROTX-MP [31] dataset is to evaluate modality bias and their generalizability when there is a substantial distributional difference in the train and test data. Following the original work [31], we train models on general datasets (FLIR [17], and CVC-14 [19]) and test models on ROTX-MP. The results are in Table 1 (Right). MSCoTDet achieves the best performance on ROTX-MP for both cases when trained on FLIR and CVC-14. When trained from FLIR, MSCoTDet achieves the highest AP (67.33 AP), which outperforms other methods by at least 10.24 AP. When trained from CVC-14, MSCoTDet achieves the highest AP (57.65 AP), which outperforms other methods by at least 22.69 AP. Such results indicate that MSCoTDet has a better ability to intervene in modality bias compared to other models.

6 Ablation Study

6.1 Effect of Using Language Models

We conduct an ablation study to evaluate the effectiveness of using language models for our framework. For the experiment, we compare MSCoTDet and three detection models: (1) ‘RGB only’, (2) ‘Thermal only’, and (3) ‘Late-fusion’. First, the ‘RGB only’, and the ‘Thermal only’ model indicate single-modal detection in the vision branch of MSCoTDet. Second, ‘Late-fusion’ is in which the single-modal detections of ‘RGB only’ and ‘Thermal only’ are fused, i.e., equivalent to the vision branch equipped with vision-driven detection of our framework. Thus, to measure the effect of using language models, our main focus is to compare ‘Late-fusion’ with MSCoTDet. The results are shown in Table 2. Our method achieves higher performance than ‘Late-fusion’ in all FLIR [17], CVC-14 [19], and ROTX-MP [31]. The results on the FLIR and CVC-14 indicate that using language models can improve the overall performance of multispectral pedestrian detectors in general datasets. Also, the results on ROTX-MP indicate that using language models can significantly improve the generalizability of multispectral pedestrian detectors, and effectively mitigate the modality bias.

6.2 Effect of the Fusion Strategy

We conduct an ablation study to validate the design choice of our fusion strategy in Section 3.4. For score-fusion, our fusion strategy adapts the NMS (Eq. 2) in the vision-driven detection (‘V’) and averaging (Eq. 1) strategy in the vision-language fusion (‘VL’), respectively. Denote the averaging strategy as ‘Avg’ and NMS as ‘Max’.

Train		FLIR		CVC-14		
Test		FLIR		CVC-14		
Method		AP (↑)		MR (↓)		
V	VL	All	Day	Night	All	
Avg	Avg	89.47	10.98	17.38	16.12	
Avg	Max	88.31	10.26	18.53	15.71	
Max	Max	89.94	8.83	17.54	14.07	
Max	Avg	90.39	6.69	13.69	10.39	

Train		FLIR		CVC-14	
Test		ROTX-MP		ROTX-MP	
Method		AP (↑)		AP (↑)	
V	VL	All	All	All	All
Avg	Avg	66.22	56.69		
Avg	Max	66.27	56.60		
Max	Max	66.31	56.02		
Max	Avg	67.33	57.65		

Table 3: Ablation study on the score-fusion strategy. We compare the 1) Avg, Avg, 2) Avg, Max, 3) Max, Max, and 4) Max, Avg strategies in the vision-driven detection (‘V’) and in the vision-language fusion (‘VL’).

Train			FLIR			CVC-14		
Test			FLIR			CVC-14		
Method			AP (↑)			MR (↓)		
V	L	VL	All	Day	Night	All		
argmax	argmax	argmax	89.49	7.56	17.64	14.00		
s-avg	argmax	argmax	89.79	8.03	15.28	12.63		
argmax	s-avg	argmax	89.83	8.32	15.39	13.31		
s-avg	s-avg	argmax	90.32	7.60	15.14	12.54		
argmax	argmax	s-avg	89.49	6.25	18.51	14.18		
s-avg	argmax	s-avg	90.32	7.63	15.19	11.99		
argmax	s-avg	s-avg	89.73	6.85	16.81	13.47		
s-avg	s-avg	s-avg	90.39	6.69	13.69	10.39		

Train			FLIR		CVC-14	
Test			ROTX-MP		ROTX-MP	
Method			AP (↑)		AP (↑)	
V	L	VL	All	All	All	All
argmax	argmax	argmax	66.10	56.97		
s-avg	argmax	argmax	66.29	56.95		
argmax	s-avg	argmax	67.03	56.90		
s-avg	s-avg	argmax	67.24	57.13		
argmax	argmax	s-avg	66.11	57.01		
s-avg	argmax	s-avg	67.28	56.99		
argmax	s-avg	s-avg	67.15	57.21		
s-avg	s-avg	s-avg	67.33	57.65		

Table 4: Ablation study on the box-fusion strategy. We experiment argmax and s-avg for each vision-driven detection (‘V’), language-driven detection (‘L’), and vision-language fusion (‘VL’).

For the comparison study, we conducted experiments on the (1) Avg, Avg, (2) Avg, Max, and (3) Max, Max fusion strategies in each vision-driven detection (‘V’) and vision-language fusion (‘VL’), respectively. We do not compare different score-fusion in the language branch, as we use our proposed method: MSCoT (Section 3.3) for fusing prediction scores. All other conditions are kept the same. The results are shown in Table 3. The Max, Avg strategy consistently performs the best in all test sets.

For box-fusion, we adapt weighted averaging (Eq. 3) for all vision-driven detection (‘V’), language-driven detection (‘L’), and vision-language fusion (‘VL’). Denote the weighted averaging strategy as ‘s-avg’. For the comparison study, we consider the NMS box fusion, denoted as ‘argmax’, and compare between a total of 8 combinations (either s-avg or max in three parts). All other conditions are kept the same as our MSCoTDet design during all experiments. The results are shown in Table 4. Applying s-avg for all V, L, and VL shows the best performance for most test cases.

7 Conclusion

In this paper, we propose a novel Multispectral Chain-of-Thought Detection (MSCoTDet) framework that incorporates Large Language Models to understand the complementary information and further enhance the fusion process in multispectral pedestrian detection. Specifically, our central design is to process the detection in two consecutive branches: the vision branch and the language branch. In the vision branch, we process single-modal detectors of the two modalities. The language branch is the key design in our work, generating text descriptions of the pedestrian in each modality and process through our proposed Multispectral Chain-of-Thought (MSCoT)

prompting, which performs a step-by-step reasoning process to detect pedestrians based on the descriptions. Then, we design Language-driven Multi-modal Fusion (LMF) to enable fusion between the vision-driven and language-driven detections processed from each branch. Extensive experiments demonstrate that our proposed method can significantly improve the performance and mitigate modality bias in multispectral pedestrian detection.

References

1. Achiam, J., Adler, S., Agarwal, S., Ahmad, L., Akkaya, I., Aleman, F.L., Almeida, D., Altenschmidt, J., Altman, S., Anadkat, S., et al.: Gpt-4 technical report. arXiv preprint arXiv:2303.08774 (2023)
2. Amari, S.i.: Backpropagation and stochastic gradient descent method. *Neurocomputing* **5**(4-5), 185–196 (1993)
3. Andersen, R.A., Buneo, C.A.: Intentional maps in posterior parietal cortex. *Annual review of neuroscience* **25**(1), 189–220 (2002)
4. Brown, T., Mann, B., Ryder, N., Subbiah, M., Kaplan, J.D., Dhariwal, P., Neelakantan, A., Shyam, P., Sastry, G., Askell, A., et al.: Language models are few-shot learners. *Advances in neural information processing systems* **33**, 1877–1901 (2020)
5. Carion, N., Massa, F., Synnaeve, G., Usunier, N., Kirillov, A., Zagoruyko, S.: End-to-end object detection with transformers (2020)
6. Cha, J., Kang, W., Mun, J., Roh, B.: Honeybee: Locality-enhanced projector for multimodal llm. arXiv preprint arXiv:2312.06742 (2023)
7. Chang, Y., Wang, X., Wang, J., Wu, Y., Yang, L., Zhu, K., Chen, H., Yi, X., Wang, C., Wang, Y., et al.: A survey on evaluation of large language models. *ACM Transactions on Intelligent Systems and Technology* (2023)
8. Chen, C., Li, R., Hu, Y., Siniscalchi, S.M., Chen, P.Y., Chng, E., Yang, C.H.H.: It’s never too late: Fusing acoustic information into large language models for automatic speech recognition. arXiv preprint arXiv:2402.05457 (2024)
9. Chen, Y.T., Shi, J., Ye, Z., Mertz, C., Ramanan, D., Kong, S.: Multimodal object detection via probabilistic ensembling. In: *European Conference on Computer Vision*. pp. 139–158. Springer (2022)
10. Chowdhery, A., Narang, S., Devlin, J., Bosma, M., Mishra, G., Roberts, A., Barham, P., Chung, H.W., Sutton, C., Gehrmann, S., et al.: Palm: Scaling language modeling with pathways. *Journal of Machine Learning Research* **24**(240), 1–113 (2023)
11. Colby, C.L., Goldberg, M.E.: Space and attention in parietal cortex. *Annual review of neuroscience* **22**(1), 319–349 (1999)
12. Corbetta, M., Shulman, G.L.: Control of goal-directed and stimulus-driven attention in the brain. *Nature reviews neuroscience* **3**(3), 201–215 (2002)
13. Dai, W., Li, J., Li, D., Tiong, A.M.H., Zhao, J., Wang, W., Li, B., Fung, P., Hoi, S.: Instructblip: Towards general-purpose vision-language models with instruction tuning (2023)
14. Das, A., Das, S., Sistu, G., Horgan, J., Bhattacharya, U., Jones, E., Glavin, M., Eising, C.: Revisiting modality imbalance in multimodal pedestrian detection. arXiv preprint arXiv:2302.12589 (2023)
15. Dollar, P., Wojek, C., Schiele, B., Perona, P.: Pedestrian detection: An evaluation of the state of the art. *IEEE transactions on pattern analysis and machine intelligence* **34**(4), 743–761 (2011)

16. Feng, G., Zhang, B., Gu, Y., Ye, H., He, D., Wang, L.: Towards revealing the mystery behind chain of thought: a theoretical perspective. *Advances in Neural Information Processing Systems* **36** (2024)
17. FLIR Systems, I.: Free teledyne flir thermal dataset for algorithm training. <https://www.flir.com/oem/adas/adas-dataset-form/> (2021), accessed: 2022-08-05
18. Girshick, R.: Fast r-cnn. In: *Proceedings of the IEEE international conference on computer vision*. pp. 1440–1448 (2015)
19. González, A., Fang, Z., Socarras, Y., Serrat, J., Vázquez, D., Xu, J., López, A.M.: Pedestrian detection at day/night time with visible and fir cameras: A comparison. *Sensors* **16**(6), 820 (2016)
20. Guan, D., Cao, Y., Yang, J., Cao, Y., Yang, M.Y.: Fusion of multispectral data through illumination-aware deep neural networks for pedestrian detection. *Information Fusion* **50**, 148–157 (2019)
21. Hasan, I., Liao, S., Li, J., Akram, S.U., Shao, L.: Generalizable pedestrian detection: The elephant in the room. In: *Proceedings of the IEEE/CVF Conference on Computer Vision and Pattern Recognition*. pp. 11328–11337 (2021)
22. He, K., Zhang, X., Ren, S., Sun, J.: Deep residual learning for image recognition. In: *Proceedings of the IEEE conference on computer vision and pattern recognition*. pp. 770–778 (2016)
23. Hessel, J., Lee, L.: Does my multimodal model learn cross-modal interactions? it’s harder to tell than you might think! arXiv preprint arXiv:2010.06572 (2020)
24. Hoffmann, J., Borgeaud, S., Mensch, A., Buchatskaya, E., Cai, T., Rutherford, E., Casas, D.d.L., Hendricks, L.A., Welbl, J., Clark, A., et al.: Training compute-optimal large language models. arXiv preprint arXiv:2203.15556 (2022)
25. Hsu, W.Y., Lin, W.Y.: Ratio-and-scale-aware yolo for pedestrian detection. *IEEE transactions on image processing* **30**, 934–947 (2020)
26. Hwang, S., Park, J., Kim, N., Choi, Y., So Kweon, I.: Multispectral pedestrian detection: Benchmark dataset and baseline. In: *Proceedings of the IEEE conference on computer vision and pattern recognition*. pp. 1037–1045 (2015)
27. Kasneci, E., Seifler, K., Küchemann, S., Bannert, M., Dementieva, D., Fischer, F., Gasser, U., Groh, G., Günemann, S., Hüllermeier, E., et al.: Chatgpt for good? on opportunities and challenges of large language models for education. *Learning and individual differences* **103**, 102274 (2023)
28. Kim, J.U., Park, S., Ro, Y.M.: Uncertainty-guided cross-modal learning for robust multispectral pedestrian detection. *IEEE Transactions on Circuits and Systems for Video Technology* **32**(3), 1510–1523 (2021)
29. Kim, J.U., Park, S., Ro, Y.M.: Uncertainty-guided cross-modal learning for robust multispectral pedestrian detection. *IEEE Transactions on Circuits and Systems for Video Technology* **32**(3), 1510–1523 (2022). <https://doi.org/10.1109/TCSVT.2021.3076466>
30. Kim, T., Lee, H.J., Ro, Y.M.: Map: Multispectral adversarial patch to attack person detection. In: *ICASSP 2022-2022 IEEE International Conference on Acoustics, Speech and Signal Processing (ICASSP)*. pp. 4853–4857. IEEE (2022)
31. Kim, T., Shin, S., Yu, Y., Kim, H.G., Ro, Y.M.: Causal mode multiplexer: A novel framework for unbiased multispectral pedestrian detection (2024)
32. Kim, T., Yu, Y., Ro, Y.M.: Defending physical adversarial attack on object detection via adversarial patch-feature energy. In: *Proceedings of the 30th ACM International Conference on Multimedia*. pp. 1905–1913 (2022)
33. Kim, T., Yu, Y., Ro, Y.M.: Multispectral invisible coating: laminated visible-thermal physical attack against multispectral object detectors using transparent low-e films. In: *Proceedings of the AAAI Conference on Artificial Intelligence*. vol. 37, pp. 1151–1159 (2023)

34. Koh, J.Y., Fried, D., Salakhutdinov, R.R.: Generating images with multimodal language models. *Advances in Neural Information Processing Systems* **36** (2024)
35. Koh, J.Y., Salakhutdinov, R., Fried, D.: Grounding language models to images for multi-modal inputs and outputs. In: *International Conference on Machine Learning*. pp. 17283–17300. PMLR (2023)
36. Li, C., Song, D., Tong, R., Tang, M.: Multispectral pedestrian detection via simultaneous detection and segmentation. *arXiv preprint arXiv:1808.04818* (2018)
37. Li, C., Song, D., Tong, R., Tang, M.: Illumination-aware faster r-cnn for robust multispectral pedestrian detection. *Pattern Recognition* **85**, 161–171 (2019)
38. Lin, T.Y., Maire, M., Belongie, S., Hays, J., Perona, P., Ramanan, D., Dollár, P., Zitnick, C.L.: Microsoft coco: Common objects in context. In: *Computer Vision–ECCV 2014: 13th European Conference, Zurich, Switzerland, September 6–12, 2014, Proceedings, Part V* 13. pp. 740–755. Springer (2014)
39. Liu, H., Li, C., Wu, Q., Lee, Y.J.: Visual instruction tuning. *Advances in neural information processing systems* **36** (2024)
40. Liu, J., Zhang, S., Wang, S., Metaxas, D.N.: Multispectral deep neural networks for pedestrian detection. *arXiv preprint arXiv:1611.02644* (2016)
41. Loshchilov, I., Hutter, F.: Decoupled weight decay regularization. *arXiv preprint arXiv:1711.05101* (2017)
42. Morvant, E., Habrard, A., Ayache, S.: Majority vote of diverse classifiers for late fusion. In: *Structural, Syntactic, and Statistical Pattern Recognition: Joint IAPR International Workshop, S+ SSPR 2014, Joensuu, Finland, August 20–22, 2014. Proceedings*. pp. 153–162. Springer (2014)
43. Nguyen, T.M., Nguyen, T., Le, T.M., Tran, T.: Gefa: early fusion approach in drug-target affinity prediction. *IEEE/ACM transactions on computational biology and bioinformatics* **19**(2), 718–728 (2021)
44. OpenAI, I.: Chatgpt-3.5 turbo api. <https://chat.openai.com/> (2023), accessed: 2024-02-29
45. OpenAI, I.: Gpt-3.5 turbo fine-tuning and api updates. <https://openai.com/blog/gpt-3-5-turbo-fine-tuning-and-api-updates> (2023), accessed: 2024-02-29
46. Ouyang, L., Wu, J., Jiang, X., Almeida, D., Wainwright, C., Mishkin, P., Zhang, C., Agarwal, S., Slama, K., Ray, A., et al.: Training language models to follow instructions with human feedback. *Advances in Neural Information Processing Systems* **35**, 27730–27744 (2022)
47. Pandeya, Y.R., Lee, J.: Deep learning-based late fusion of multimodal information for emotion classification of music video. *Multimedia Tools and Applications* **80**, 2887–2905 (2021)
48. Peng, Z., Wang, W., Dong, L., Hao, Y., Huang, S., Ma, S., Ye, Q., Wei, F.: Grounding multimodal large language models to the world. In: *The Twelfth International Conference on Learning Representations* (2023)
49. Qingyun, F., Dapeng, H., Zhaokui, W.: Cross-modality fusion transformer for multispectral object detection. *arXiv preprint arXiv:2111.00273* (2021)
50. Qingyun, F., Dapeng, H., Zhaokui, W.: Cross-modality fusion transformer for multispectral object detection (2022)
51. Shi, F., Suzgun, M., Freitag, M., Wang, X., Srivats, S., Vosoughi, S., Chung, H.W., Tay, Y., Ruder, S., Zhou, D., et al.: Language models are multilingual chain-of-thought reasoners. *arXiv preprint arXiv:2210.03057* (2022)
52. Shutova, E., Kiela, D., Maillard, J.: Black holes and white rabbits: Metaphor identification with visual features. In: *Proceedings of the 2016 conference of the North American chapter of the association for computational linguistics: Human language technologies*. pp. 160–170 (2016)

53. Snoek, C.G., Worring, M., Smeulders, A.W.: Early versus late fusion in semantic video analysis. In: Proceedings of the 13th annual ACM international conference on Multimedia. pp. 399–402 (2005)
54. Touvron, H., Lavril, T., Izacard, G., Martinet, X., Lachaux, M.A., Lacroix, T., Rozière, B., Goyal, N., Hambro, E., Azhar, F., et al.: Llama: Open and efficient foundation language models. arXiv preprint arXiv:2302.13971 (2023)
55. Tsimpoukelli, M., Menick, J.L., Cabi, S., Eslami, S., Vinyals, O., Hill, F.: Multimodal few-shot learning with frozen language models. *Advances in Neural Information Processing Systems* **34**, 200–212 (2021)
56. Tziafas, G., Kasaei, H.: Early or late fusion matters: Efficient rgb-d fusion in vision transformers for 3d object recognition. In: 2023 IEEE/RSJ International Conference on Intelligent Robots and Systems (IROS). pp. 9558–9565. IEEE (2023)
57. Wagner, J., Fischer, V., Herman, M., Behnke, S., et al.: Multispectral pedestrian detection using deep fusion convolutional neural networks. In: ESANN. vol. 587, pp. 509–514 (2016)
58. Wang, X., Wei, J., Schuurmans, D., Le, Q., Chi, E., Narang, S., Chowdhery, A., Zhou, D.: Self-consistency improves chain of thought reasoning in language models. arXiv preprint arXiv:2203.11171 (2022)
59. Wei, J., Wang, X., Schuurmans, D., Bosma, M., Xia, F., Chi, E., Le, Q.V., Zhou, D., et al.: Chain-of-thought prompting elicits reasoning in large language models. *Advances in Neural Information Processing Systems* **35**, 24824–24837 (2022)
60. Workshop, B., Scao, T.L., Fan, A., Akiki, C., Pavlick, E., Ilić, S., Hesslow, D., Castagné, R., Luccioni, A.S., Yvon, F., et al.: Bloom: A 176b-parameter open-access multilingual language model. arXiv preprint arXiv:2211.05100 (2022)
61. Wu, Y., Kirillov, A., Massa, F., Lo, W.Y., Girshick, R.: Detectron2. <https://github.com/facebookresearch/detectron2> (2019)
62. Xu, D., Ouyang, W., Ricci, E., Wang, X., Sebe, N.: Learning cross-modal deep representations for robust pedestrian detection. In: Proceedings of the IEEE conference on computer vision and pattern recognition. pp. 5363–5371 (2017)
63. Yao, Y., Mihalcea, R.: Modality-specific learning rates for effective multimodal additive late-fusion. In: Findings of the Association for Computational Linguistics: ACL 2022. pp. 1824–1834 (2022)
64. Zhang, H., Fromont, E., Lefevre, S., Avignon, B.: Multispectral fusion for object detection with cyclic fuse-and-refine blocks. In: 2020 IEEE International conference on image processing (ICIP). pp. 276–280. IEEE (2020)
65. Zhang, J., Khayatkhoei, M., Chhikara, P., Iliovski, F.: Visual cropping improves zero-shot question answering of multimodal large language models. arXiv preprint arXiv:2310.16033 (2023)
66. Zhang, L., Liu, Z., Zhang, S., Yang, X., Qiao, H., Huang, K., Hussain, A.: Cross-modality interactive attention network for multispectral pedestrian detection. *Information Fusion* **50**, 20–29 (2019)
67. Zhang, L., Zhu, X., Chen, X., Yang, X., Lei, Z., Liu, Z.: Weakly aligned cross-modal learning for multispectral pedestrian detection. In: Proceedings of the IEEE/CVF international conference on computer vision. pp. 5127–5137 (2019)
68. Zhang, Z., Zhang, A., Li, M., Smola, A.: Automatic chain of thought prompting in large language models. arXiv preprint arXiv:2210.03493 (2022)
69. Zhang, Z., Zhang, A., Li, M., Zhao, H., Karypis, G., Smola, A.: Multimodal chain-of-thought reasoning in language models. arXiv preprint arXiv:2302.00923 (2023)
70. Zhou, K., Chen, L., Cao, X.: Improving multispectral pedestrian detection by addressing modality imbalance problems. In: Computer Vision–ECCV 2020: 16th European Conference, Glasgow, UK, August 23–28, 2020, Proceedings, Part XVIII 16. pp. 787–803. Springer (2020)

71. Zhu, D., Chen, J., Shen, X., Li, X., Elhoseiny, M.: Minigt-4: Enhancing vision-language understanding with advanced large language models. arXiv preprint arXiv:2304.10592 (2023)
72. Zong, Z., Song, G., Liu, Y.: Detsr with collaborative hybrid assignments training. In: Proceedings of the IEEE/CVF international conference on computer vision. pp. 6748–6758 (2023)

Supplementary Material

A Training Data for MSCoT

Examples of Training Data. We provide examples of the training data for Multi-spectral Chain-of-Thought (MSCoT, Section 3.3 in the manuscript). The training data contains descriptions of RGB and thermal images, rationale, and prediction scores for training the Large Language Model. First, we obtain the textual descriptions of RGB and thermal images using the Multi-modal Large Language Model (MLLM) [1], illustrated in the top part of Figure 1. Here, the MLLM gets pre-processed images as the input and outputs their corresponding textual descriptions. We use the ChatGPT-vision (GPT-4V) for the MLLM. Then we prompt the GPT-3.5 [44] consisting of rationale, and prediction scores for our MSCoT, which the prompts are in blue texts in Figure 1. The following answers are obtained by prompting the GPT-3.5 independently with these prompts, and we merge the answers to make the training data. Figure 1 shows an example of training data. Then with these data, we fine-tune the model answer based on a chain of prompts. The training data are manually selected with high-quality answers. 50 training data from the FLIR training images are used for fine-tuning MSCoT of the FLIR model. Also, we made 50 training data using the CVC-14 training images for MSCoT of the CVC-14 model. Note that images from ROTX-MP are not used for making training data for MSCoT because it violates the evaluation setting for ROTX-MP. The evaluation rule on ROTX-MP is to use models trained on general datasets (e.g., FLIR and CVC-14) and test those models on ROTX-MP. Thus our MSCoT does not violate the evaluation rule on ROTX-MP. An example of our training data are illustrated in Figure 1 below.

Training Detail. We use the ChatGPT-3.5 (GPT-3.5) API [44], provided by the OpenAI developer platform. Using the fine-tuning module provided on the GPT official website [45], we trained GPT-3.5 API with our training data. The official document for GPT-3.5 [45] recommends training 50 samples for fine-tuning the model, and we utilized a total of 50 training samples for each FLIR and CVC-14 model.

B Related Work

B.1 Multispectral Pedestrian Detection

Dataset. Different from standard pedestrian detection, multispectral pedestrian detection aims to detect pedestrians using RGB and thermal images. The KAIST [26] dataset is one of the first benchmarks for multispectral pedestrian detection, containing well-aligned RGB and thermal images with pedestrians captured from all daytime/nighttime. The FLIR [17] dataset is a newer benchmark, offering higher image quality and resolution than KAIST [26]. While the KAIST [26] and FLIR [17] datasets provide a benchmark for well-aligned RGB-thermal images, the CVC-14 [19]

dataset introduces a benchmark that largely contains misaligned RGB-thermal images, highlighting the challenges due to modality misalignments. Furthermore, the ROTX-MP [31] dataset provides a challenging benchmark, evaluating modality biases in multispectral pedestrian detection. In other multispectral pedestrian datasets (e.g., KAIST, CVC-14, and FLIR), pedestrians always statistically co-occur with their thermal signatures [31]. On the other hand, ROTX-MP mainly contains thermal-obscured data, in which the thermal signatures of pedestrians are absent due to the intermediate obstacles (e.g., windows and heat-insulating clothes). Modality biases are evaluated under the setting that training the models on general datasets (e.g., KAIST, CVC-14, and FLIR) and testing their performance on ROTX-MP.

Model. To solve these challenges presented in multispectral pedestrian detection, various methods have been proposed [9, 28, 36, 40, 49, 57]. To alleviate modality misalignment problems, Kim et al.(2022) [29] proposed an uncertainty-aware feature fusion (UFF) network. UFF first estimates the uncertainty value of each modality feature and assigns different weights in the fusion process. Cross-Modality Fusion Transformer [50] enhances feature fusion by designing a new cross-modality fusion mechanism based on self-attention. ProbEn [9] propose a late-fusion-based strategy, which probabilistically ensembles prediction scores and bounding boxes obtained from single-modal detectors of different modalities. Lastly, the Causal Mode Multiplexer (CMM) [31] framework is proposed to mitigate modality bias via counterfactual intervention and improve the performance on thermal-obscured data.

B.2 Large Language Model

Large language models (LLMs) excel in natural language processing (NLP) and generation by training on vast amounts of text data [4, 10, 24, 46, 54, 60]. These features and advantages offer innovative applicability across more general areas of intelligence. Multimodal large language models (MLLMs), such as LLaVA [39], MiniGPT-4 [71], and InstructBLIP [13], rely on the high-level understanding and recognition of linguistic and visual content that LLMs possess. In visual grounding [34, 35, 48], MLLMs can comprehend the context within an image by identifying objects, attributes, and the overall scene. They excel at linking these visual contextual elements with textual descriptions in semantic space. Large-scale language models can process and generate multimodal data across various input formats, enabling applications in diverse fields. Recently, the ability to leverage LLM’s semantic understanding capabilities to model and understand continuous streams of thought has gained traction. ScienceQA [6, 69], a benchmark task based on scientific knowledge for natural language understanding and question answering, highlights the advantages of language ability. LLMs understand questions through a step-by-step approach called Chain-of-Thought (CoT) [59] and make inferences based on learned knowledge. CoT aggregates and synthesizes given knowledge to provide new insights and can improve issues (e.g., hallucination) commonly encountered in answering difficult questions.

C Implementation Detail

For all models, the setting is kept the same across training CVC [19], and FLIR [17] datasets.

CMM [31]: The CMM framework is based on the Uncertainty-guided model [29], with the FPN architecture with ResNet-50 [22] as backbone networks. Specifically, we use the pytorch library and stochastic gradient descent (SGD) for optimization, synchronizing the process across 4 GTX 1080 Ti GPUs. Each GPU handles 2 images, resulting in a total of 8 images per mini-batch. The model is trained for 2 epochs. The learning rate is initialized at 0.007 during the initial 1 epoch and subsequently applied a 0.1 learning rate decay for the final epoch. We configured the number of Region of Interests (RoIs) per image to $N=300$. We apply switchable Total Indirect Effect (sTIE) for every ROI and compute the prediction score. The final predictions are made through the Non-Maximum Suppression (NMS) process. We use the code provided by the authors, with the same settings as the original paper [31].

ProbEn [9]: ProbEn train two single-modal detectors based on Faster R-CNN [18] with Detectron 2 [61]. We used 2 NVIDIA RTX3090 GPUs with SGD [2] optimizer with learning rate $5e-3$. Image flip and resize is applied for data augmentation. Also, we pre-process the RGB and thermal images by subtracting the mean input value, which is (103.53, 116.28, 123.67) and (135.438) for each RGB and thermal images. The min value of the input pixel is 0 and max value is 255 for each channel. We adopt the 'ProbEn' score fusion and 'v-avg' box fusion because such combinations are shown the most effective in the original paper [9]. Also, we adopt the E+M+T ensemble version when experimenting on the FLIR dataset, indicating that early-fusion, mid-fusion, and thermal single-modal detectors are ensembled. We adopt the R+M+T ensemble version when experimenting on the CVC-14 dataset, indicating that mid-fusion, RGB, and thermal single-modal detectors are ensembled. The single-modal detectors are pre-trained on the COCO dataset [38] and then trained in the FLIR or CVC-14 dataset, same as the original paper.

Kim et al. [29]: We train the model for 3 epochs. The learning rate is initialized at 0.006 during the initial 2 epochs and subsequently applied a 0.1 learning rate decay for the final epoch. As this model is the baseline model of CMM, we set the other hyper-parameters the same as CMM. We use the code provided by the authors, with the same settings as the original paper [29].

Halfway Fusion [40]: We use the Faster-RCNN [18] as the base model and train the model for 3 epochs. The learning rate is initialized at 0.008 during the initial 2 epochs and subsequently applied a 0.1 learning rate decay for the final epoch. The SGD optimizer is used.

CFT [50]: We use the same setting as the original paper. The initial learning rate is 0.01 with a momentum of 0.937, and weight decay 0.0005. Batch size is 32 and the model is trained for 200 epochs and the YOLO-v5 weight trained on the COCO dataset is used for weight initialization. We used the official code from GitHub.

Algorithm 1 Cross-aligned Pedestrian Description Generation (CPDG)

-
- 1: **Input:** An RGB image X_{RGB} , an thermal image X_T , prediction scores S_{RGB} , S_T and bounding boxes B_{RGB} , B_T .
 - 2: **Require:** Input text prompts p_{RGB} , p_T , and IoU threshold τ . Detection pairing module $DPair(\cdot)$, Visual Crop & Mark module $VCM(\cdot)$. A pre-trained multimodal large language model $MLLM(\cdot)$.
 - 3: **Output:** A set of RGB descriptions D_{RGB} , a set of thermal descriptions D_T , and paired detections S^{paired} , B^{paired} .
 - 4:
 - 5: **procedure** $CPDG(X_{RGB}, X_T, S_{RGB}, S_T, B_{RGB}, B_T; p_{RGB}, p_T, \tau)$
 - 6: $S^{paired}, B^{paired} \leftarrow DPair(B_{RGB}, B_T, S_{RGB}, S_T; \tau)$.
 - 7: $X_{RGB}^{VCM} \leftarrow VCM(X_{RGB}, B^{paired})$, $X_T^{VCM} \leftarrow VCM(X_T, B^{paired})$.
 - 8: **initialize** list $D_{RGB} \leftarrow \phi$, $D_T \leftarrow \phi$.
 - 9: **for** all images x_{RGB}^{VCM} in X_{RGB}^{VCM}
 - 10: $d_{RGB} = MLLM(x_{RGB}^{VCM}; p_{RGB})$.
 - 11: Append the text description d_{RGB} to the list D_{RGB} .
 - 12: **end for**
 - 13: **for** all images x_T^{VCM} in X_T^{VCM}
 - 14: $d_T = MLLM(x_T^{VCM}; p_T)$.
 - 15: Append the text description d_T to the list D_T .
 - 16: **end for**
 - 17: **return** $D_{RGB}, D_T, S^{paired}, B^{paired}$.
 - 18: **end procedure**
-

D Detailed Algorithm**D.1 Cross-aligned Pedestrian Description Generation**

The detailed algorithm of Cross-aligned Pedestrian Description Generation is described in Algorithm 1. Denote the procedure $CPDG(\cdot)$. $CPDG(\cdot)$ gets inputs: An RGB image X_{RGB} , an thermal image X_T , prediction scores S_{RGB} , S_T and bounding boxes B_{RGB} , B_T . And $CPDG(\cdot)$ requires input text prompts p_{RGB} , p_T , and the IoU threshold τ . Detection pairing module $DPair(\cdot)$, Visual Crop & Mark module $VCM(\cdot)$. A pretrained multimodal large language model $MLLM(\cdot)$. Then $CPDG(\cdot)$ outputs a set of RGB descriptions D_{RGB} , a set of thermal descriptions D_T , and paired detections S^{paired} , B^{paired} .

The first process is to produce paired detections S^{paired} , B^{paired} through the detection pairing module $Dpair(\cdot)$, line 6 in Algorithm 1. The detailed process of $Dpair(\cdot)$ is described in Algorithm 2. Then, using the paired bounding boxes B^{paired} , the Visual Crop & Mark module $VCM(\cdot)$ produces pre-processed images X_{RGB}^{VCM} and X_T^{VCM} . For each image in $x_{RGB}^{VCM} \in X_{RGB}^{VCM}$, the pre-trained $MLLM(\cdot)$ produces text descriptions d_{RGB} , which is appended to the set D_{RGB} . Similarly, each image in $x_T^{VCM} \in X_T^{VCM}$, the pre-trained $MLLM(\cdot)$ produces text descriptions d_T , and is appended to the set D_T . Finally, $CPDG(\cdot)$ outputs sets of textual descriptions D_{RGB} , D_T , and paired detections S^{paired} and B^{paired} . We describe each Detection Pairing, Visual Crop & Mark module in the following.

Algorithm 2 Detection Pairing (DPair)

-
- 1: **Input:** Prediction scores S_{RGB}, S_T , Bounding boxes B_{RGB}, B_T .
 - 2: **Require:** An IoU threshold τ .
 - 3: **Output:** Paired bounding boxes B^{paired} , paired prediction scores S^{paired} .
 - 4:
 - 5: **procedure** DPair($B_{RGB}, B_T, S_{RGB}, S_T; \tau$)
 - 6: **initialize** lists $B \leftarrow B_{RGB} \cup B_T, S \leftarrow S_{RGB} \cup S_T, B^{paired} \leftarrow \phi$, and $S^{paired} \leftarrow \phi$.
 - 7: Find the box $b_{max} \in B$ of the highest prediction score.
 - 8: Find boxes $D \in B$ overlapping with b_{max} , of IoU ($> \tau$) in the opposite modality.
 - 9: Find the box $b_{pair} \in D$ of the highest IoU value.
 - 10: If D is empty, then $b_{pair} \leftarrow b_{max}$ and $s_{pair} \leftarrow s_{max}$.
 - 11: Append (b_{max}, b_{pair}) to B^{paired}
 - 12: Append (s_{max}, s_{pair}) to S^{paired} .
 - 13: Remove b_{max} and b_{pair} from B and s_{max} and s_{pair} from S
 - 14: Repeat this process until B and S are empty.
 - 15: **return** B^{paired}, S^{paired}
 - 16: **end procedure**
-

D.2 Detection Pairing

Due to the misalignment between RGB and thermal images, we often need to guide MLLMs to make descriptions based on different image regions in RGB and thermal images for the same pedestrians. Our strategy is to find the detection pairs from the single-modal detections (e.g., bounding boxes) that belong to the same pedestrians and provide this information to the MLLM. We design a Detection Pairing module to do this. Although bounding boxes representing the same pedestrian can have different coordinates in different modalities, still they will contain highly overlapping areas in the images, and those boxes will have large values of IoUs (Intersection-of-Unions). Specifically, for the i -th bounding box $b_{i,m}$ in bounding boxes B_m , obtained from the single-modal detector in the m modality (m is either RGB or thermal: T), we aim to find the bounding box from B_{m^c} , in the opposite modality m^c that corresponds to the same pedestrian. To this end, we compute the IoU value between $b_{i,m}$ across all bounding boxes in B_{m^c} , and find the box that has the highest IoU value, e.g., b_{j,m^c} , with $b_{i,m}$. Here, we only consider the boxes with IoU values above the IoU threshold τ . With indices i and j , we can find a pair of the prediction scores $s_{i,m}$ and s_{j,m^c} that belong to the same pedestrian. We call such tuples $(b_{i,m}, b_{j,m^c})$ and $(s_{i,m}, s_{j,m^c})$ as the "paired detection". When all IoU values are under the IoU threshold τ , this means that there are no boxes in B_{m^c} that correspond to the same pedestrian and $b_{i,m}$ can not find a pair. Such cases can occur at nighttime or in thermal-obscured scenarios where the pedestrian is detected by only one modality. In this case, we override the value of $b_{i,m}$ and $s_{i,m}$ to the opposite modality, making pairs of $(b_{i,m}, b_{i,m})$ and $(s_{i,m}, s_{i,m})$. Iterating this process for over all bounding boxes in B_m and B_{m^c} (i.e., B_{RGB} and B_T) allows us to obtain a set of paired detections B^{paired} and S^{paired} . Denote the Detection Pairing Module as a function $DPair(\cdot)$ with respect to inputs B_{RGB}, B_T, S_{RGB} , and S_T , which indicate bounding boxes and prediction scores obtained from RGB and thermal single-modal detectors, respectively. The inputs and

Algorithm 3 Visual Crop & Mark (VCM)

```

1: Input: An image  $X$ , and bounding boxes  $B$ .
2: Output: Pre-processed images  $X^{VCM}$ .
3:
4: procedure VCM( $X, B$ )
5:   initialize  $X^{VCM} \leftarrow \phi$ .
6:   for all bounding boxes  $b$  in  $B$ 
7:     Draw a green box at bounding box  $b$  in the image  $X$ .
8:     Crop the image  $X$  around the bounding box  $b$  such that the width and height of the
9:     cropped image  $X_c$  are twice as the width and height of  $b$ .
10:    Append the cropped image  $X_c$  to  $X^{VCM}$ .
11:   end for
12:   return  $X^{VCM}$ 
13: end procedure

```

outputs of $DPair(\cdot)$ can be represented as:

$$S^{paired}, B^{paired} = DPair(B_{RGB}, B_T, S_{RGB}, S_T; \tau), \quad (1)$$

where τ indicates an IoU threshold. We set this value to 0.5, the standard value used in the object detection task.

D.3 Visual Crop & Mark

The Visual Crop & Mark module performs very simple image pre-processing. First, an image X and bounding boxes B are given as input. Note that B represents the locations of pedestrians in image X . For each bounding box, $b \in B$, a green box is drawn in the image X . Then, the image X is cropped around the bounding box b so that the width and height of the cropped image X_c are twice as b . This process is iterated for all bounding boxes $b \in B$, and pre-processed images X^{VCM} are obtained. The detailed algorithm is described in Algorithm 3.

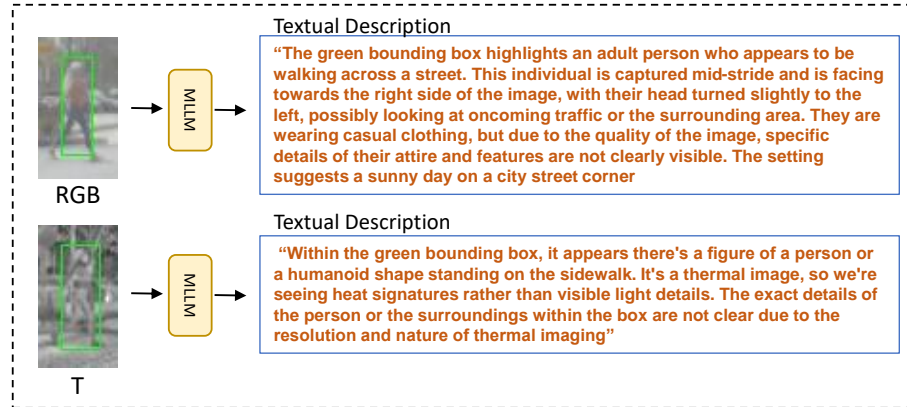
E Visualized Result

In this section, we provide visualized detections of MSCoTDet (Ours) compared to the conventional model [31] on the ROTX-MP [31], FLIR [17], and CVC-14 [19] datasets.

ROTX-MP. Figure 5 to Figure 4 show the visualized detections on the ROTX-MP [31] dataset. The conventional model [31] fails to detect thermal-obscured pedestrians in many cases. On the other hand, MSCoTDet achieves accurate detections of these pedestrians. Although MSCoTDet produces a low prediction score S_T^F from the thermal single-modal detector, the high prediction score from the language branch raises the overall prediction score S_{LMF} above the detection threshold of 0.5.

FLIR and CVC-14. Figure 5 show the visualized detections on the FLIR [17] and CVC-14 [19] datasets. Figure 5 show that MSCoTDet (Ours) can achieve more accurate detection on small-scale pedestrians, misaligned pedestrians, and objects that are likely to be detected as pedestrians because of their similar appearance to pedestrians in the thermal image.

Pre-processed Images and Their Textual Descriptions



Training Data for Fine-tuning the LLM

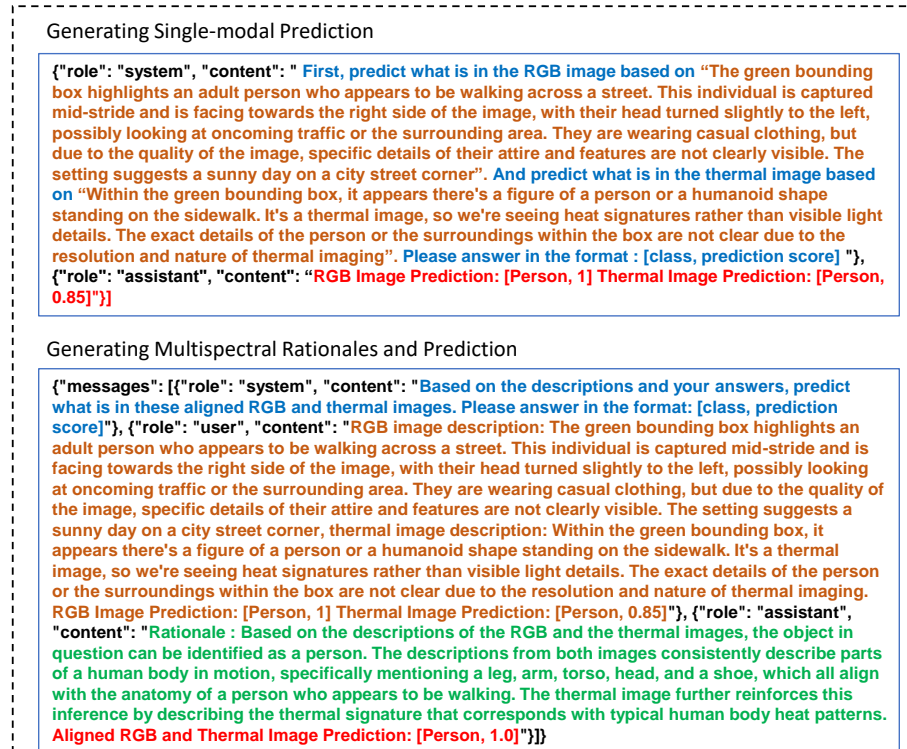


Fig. 1: (Top): Textual descriptions of an RGB and thermal image generated by a Multi-modal Large Language Model (MLLM). We use the ChatGPT-vision (GPT-4V) [1] API for the MLLM. (Bottom) Corresponding training data for fine-tuning the Large Language Model (LLM) to process Multispectral Chain-of-Thought (MSCoT). We use the ChatGPT-3.5 (GPT-3.5) API for the LLM and fine-tune them with our training data.

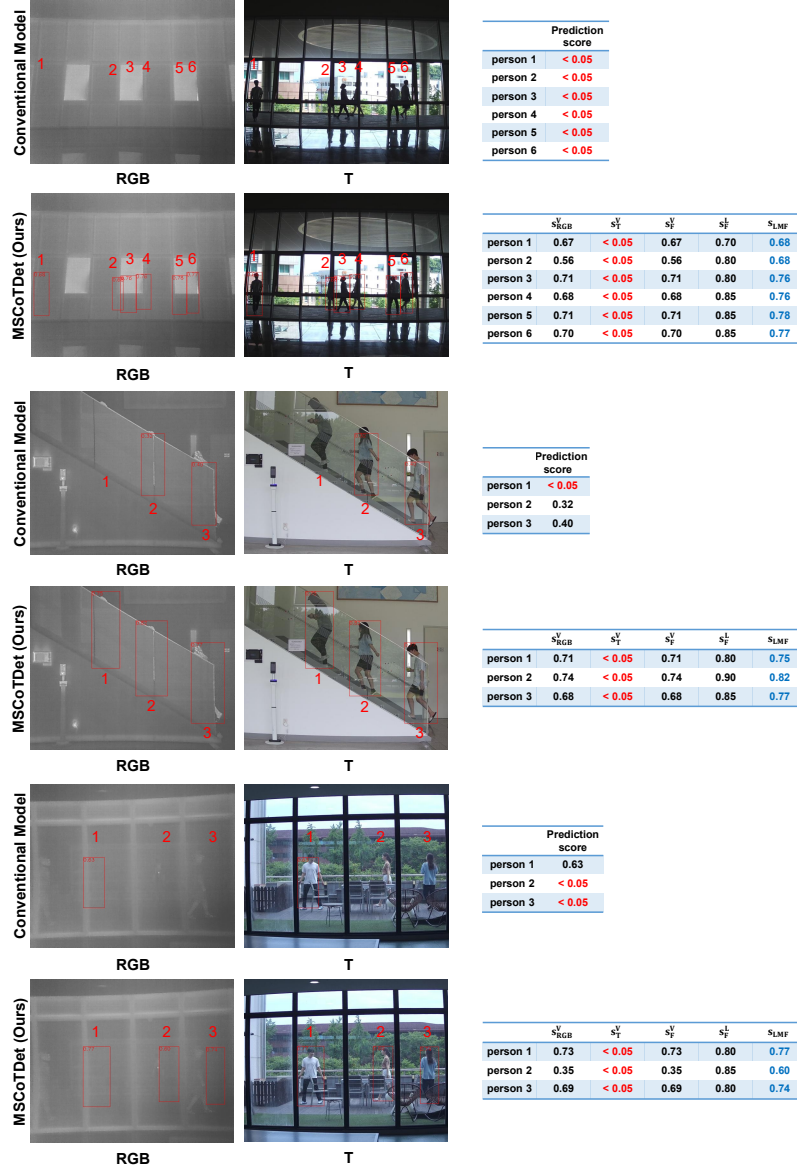


Fig. 2: Visualized detections of a conventional model [31] and MSCoTDet (Ours) on the ROTX-MP [31] dataset. MSCoTDet achieves higher prediction scores (s_{LMF}) compared to the conventional model, enabling the detection of thermal-obscured pedestrians. s_{RGB}^V , s_T^V denote prediction scores from RGB and thermal single-modal detectors, s_F^V denote the fused prediction score from the visual branch, and denote s_F^L the fused prediction score from the language branch, respectively. Only the detections with prediction scores above the threshold 0.3 are visualized.

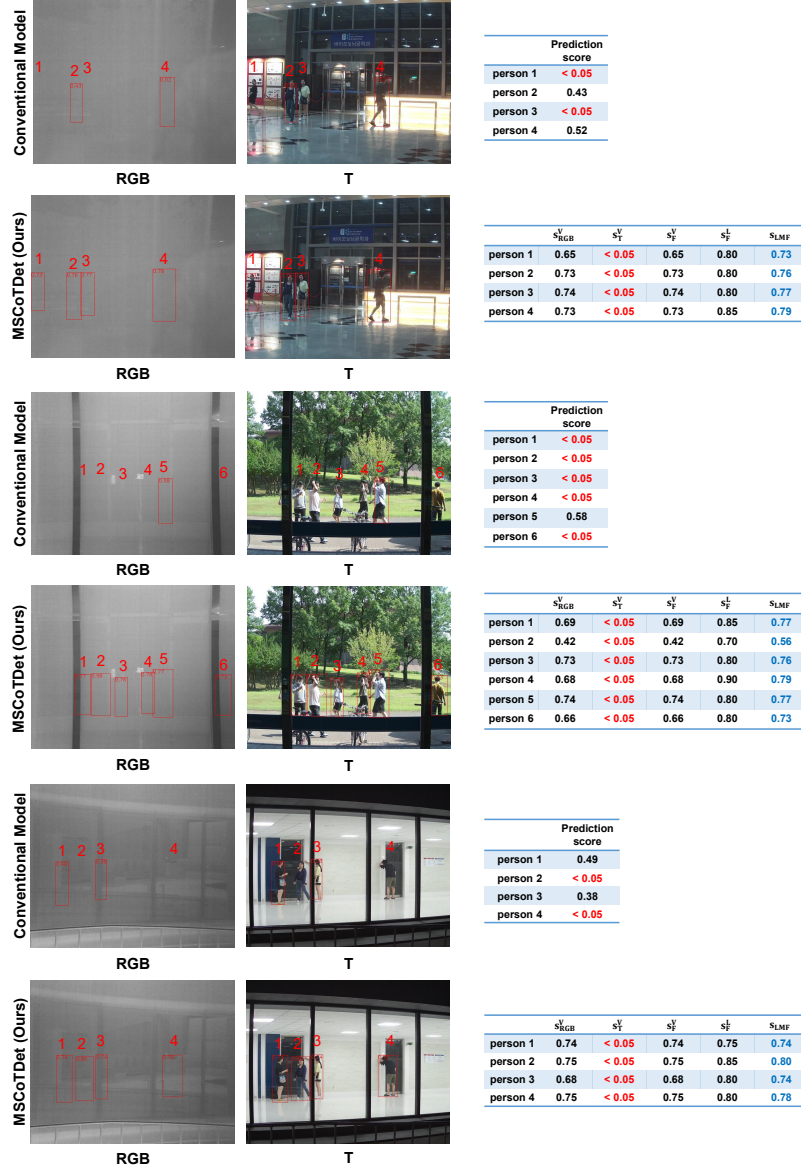


Fig. 3: Visualized detections of a conventional model [31] and MSCoTDet (Ours) on the ROTX-MP [31] dataset. MSCoTDet achieves higher prediction scores (S_{LMF}) compared to the conventional model, enabling the detection of thermal-obscured pedestrians. S_{RGB}^V , S_T^V , S_F^V , and S_F^L denote prediction scores from RGB and thermal single-modal detectors, fused prediction score from the visual branch, and fused prediction score from the language branch, respectively. Only the detections with prediction scores above the threshold 0.3 are visualized.

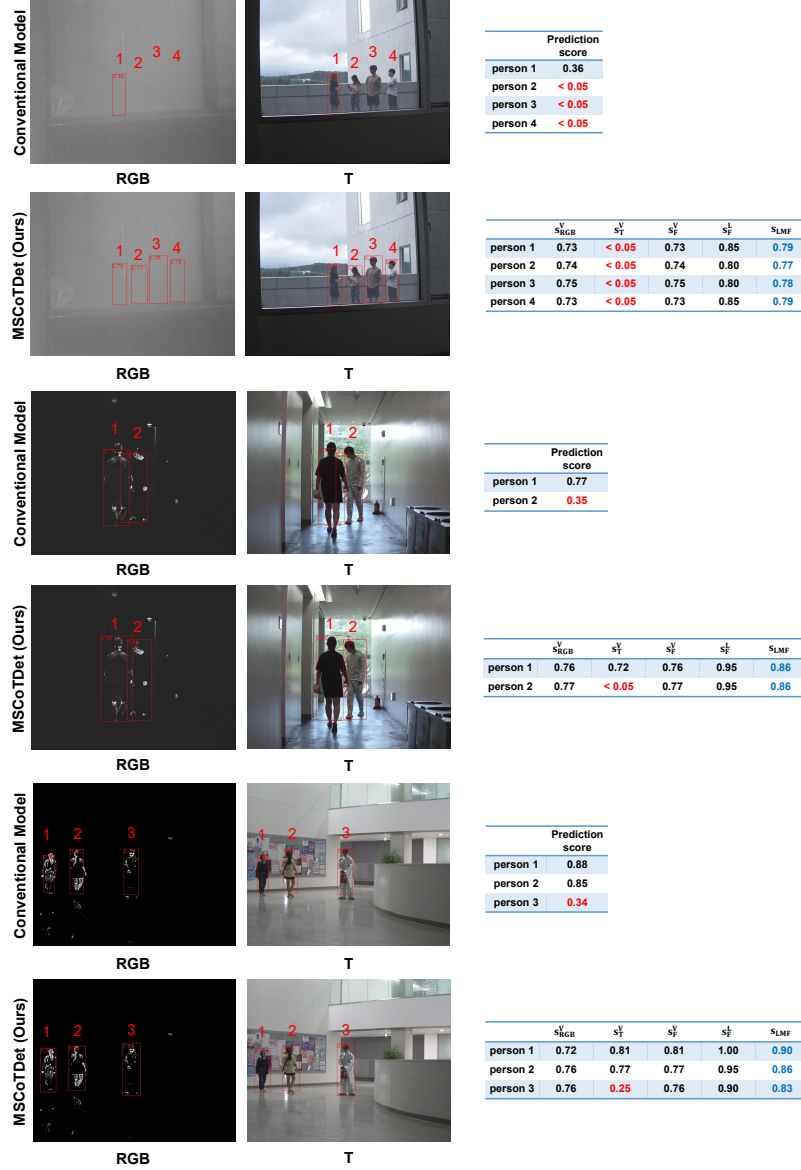


Fig. 4: Visualized detections of a conventional model [31] and MSCoTDet (Ours) on the ROTX-MP [31] dataset. MSCoTDet achieves higher prediction scores (s_{LMF}) compared to the conventional model, enabling the detection of thermal-obsured pedestrians. s_{RGB}^V , s_T^V , s_F^V , and s_F^L denote prediction scores from RGB and thermal single-modal detectors, fused prediction score from the visual branch, and fused prediction score from the language branch, respectively. Only the detections with prediction scores above the threshold 0.3 are visualized.

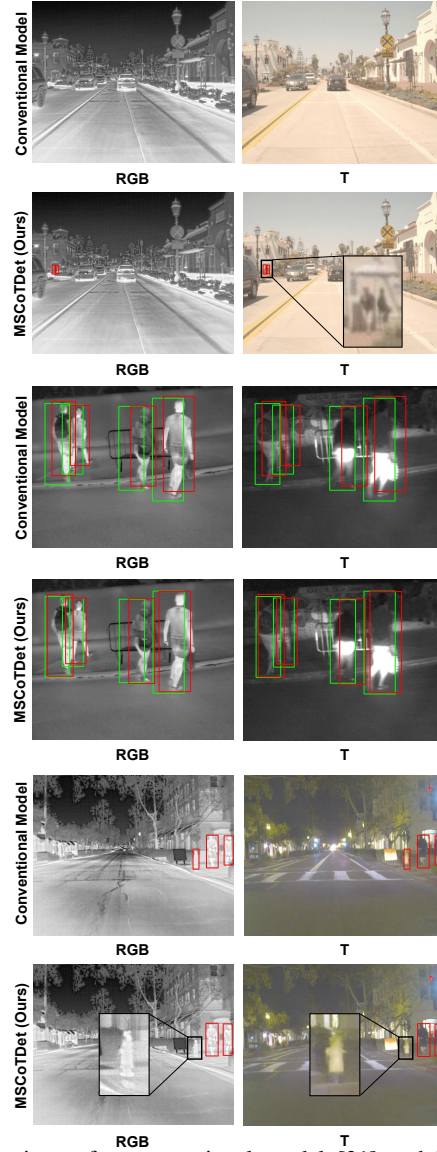


Fig. 5: Visualized detections of a conventional model [31] and MSCoTDet (Ours) on the FLIR [17] and CVC-14 [19] dataset. (Top): MSCoTDet can achieve accurate detection of small-scale pedestrians. (Middle): MSCoTDet produces bounding boxes (red) more closely to the ground-truth labels (green). (Bottom): MSCoTDet can make accurate detection on objects (e.g., fireplugs) that are likely to be detected as pedestrians, which have a similar appearance to pedestrians in the thermal image. The conventional model falsely detects the fireplug as a pedestrian. Only the detections with prediction scores above the threshold 0.3 are visualized.